

Black hole masses of weak emission line quasars based on continuum fit method

MARCIN MARCULEWICZ¹ AND MAREK NIKOLAJUK¹¹University of Białystok, Faculty of Physics, Ciołkowskiego 1L Street, 15-245 Białystok, Poland

ABSTRACT

We studied optical-ultraviolet spectral energy distribution of 10 weak emission-line quasars (WLQs) which lie at redshifts $z = 0.19$ and $1.43 < z < 3.48$. The theoretical models of their accretion disk continua are created based on the Novikov-Thorne equations. It allows us to estimate masses of their supermassive black holes (M_{BH}) and accretion rates. We determined the virial factor for WLQs and note its anti-correlation with the full width at half maximum ($FWHM$) of $H\beta$ emission-line ($f \propto FWHM^\alpha$, $\alpha = -1.34 \pm 0.37$). By comparison with the previously estimated BH masses, the underestimation of M_{BH} is noticed with a mean factor 4-5 which depends on the measured full width. We proposed the new formula to estimate M_{BH} in WLQs based on their observed $FWHM(H\beta)$ and luminosities at 5100\AA . In our opinion, WLQs are also normal quasars visible in a reactivation stage.

Keywords: black hole physics - galaxies: active - galaxies: nuclei - line: profiles - quasars: general

1. INTRODUCTION

Weak emission-line quasars (WLQs) are unsolved puzzle in the model of active galactic nuclei (AGN). Typical equivalent width (EW) of C IV emission line is extremely weak ($\lesssim 10\text{\AA}$) compared to normal quasars and very weak or absent in $\text{Ly}\alpha$ emission (Fan et al. 1999; Diamond-Stanic et al. 2009). Diamond-Stanic et al. (2009) concluded that WLQs have optical continuum properties similar to normal quasars, although $\text{Ly}\alpha + \text{N V}$ line luminosities are significantly weaker, by a factor of 4. An explanation for the weak or absent emission lines has not been found so far. Probable explanations include a radiatively inefficient accretion flow (Yuan & Narayan 2004) and a cold accretion disk (Laor & Davis 2011) with a small accretion rate. An extremely high accretion rate where we have inefficient photoionized flux is proposed by Leighly et al. (2007a,b). Parallel to that Wu et al. (2011) postulate presence of shielding gas between the accretion disk and a Broad Line Region (BLR), which could absorb the high-energy ionizing photons from the accretion disk. The last but not least, model suggests an unusual BLR i.e., anemic in construction and gas abundance (Shemmer et al. 2010; Nikolajuk & Walter 2012). This explanation supports the idea that WLQs can also be in the early stage of

AGN evolution (Hryniewicz et al. 2010; Liu & Zhang 2011; Bañados et al. 2014; Meusinger & Balafkan 2014). Several works about X-ray properties of WLQs have recently appeared (e.g. Wu et al. 2011, 2012a; Ni et al. 2018; Marlar et al. 2018). Conclusion arising from these works is that WLQs are more likely X-ray weaker (about half of them) than normal quasars. For example, Ni et al. (2018) mentioned that 7 of the 16 WLQs in their sample are X-ray weak. Luo et al. (2015) suggested that it may be caused from the shielding gas which prevents the observer to see central X-ray emitting region.

Knowledge about the values of black hole (BH) masses and the accretion rates is crucial in understanding an accretion flows phenomena. The most robust technique is the reverberation mapping method (RM, Blandford & McKee 1982; Peterson 1993, 2014; Fausnaugh et al. 2017; Bentz & Manne-Nicholas 2018; Shen et al. 2019). The method is based on the study of the dynamics surrounding the black hole gas. In this way, we are able to determine the supermassive black hole (SMBH) mass:

$$M_{\text{BH}} = \frac{v_{\text{BLR}}^2 R_{\text{BLR}}}{G} = f \frac{FWHM^2 R_{\text{BLR}}}{G} \quad (1)$$

where M_{BH} is the black hole mass, G - the gravitational constant, R_{BLR} is a distance between the SMBH and a cloud in the broad line region (BLR). v_{BLR} is a velocity of the cloud inside the BLR. This speed is unknown and we express our lack of knowledge in the form of the Full Width Half Maximum ($FWHM$) of an emission-line and f - the virial factor, which describes a distribution of the

BLR clouds. In the RM the R_{BLR} is determined as the time delay between the continuum change and the BLR response. This technique requires a significant number of observations. The modification of this method is the single-epoch virial BH mass estimator (see Shen 2013, for review). The correlation between R_{BLR} and continuum luminosity (νL_ν) is observed (Kaspi et al. 2005; Bentz et al. 2009) and incorporated in Eq. (1). Thus, the method is powerful and eagerly used because of its simplicity (Kaspi et al. 2000; Peterson et al. 2004; Vestergaard & Peterson 2006; Plotkin et al. 2015). The non-dynamic method, which is the spectra disk-fitting method, is based on well grounded model of emission from an accretion disk (AD) surrounded black hole (e.g. Shakura & Sunyaev 1973; Novikov & Thorne 1973). The most important parameter in such models is the mass of black hole and the accretion rate. The spin of the black hole and the viewing angle are also taken into account. In this technique, a SED of an AGN is fitted to the model and one is able to constrain these four parameters. More advanced disk spectra models, which take into account an irradiation effect, limb-darkening/brightening effects, the departure from a blackbody due to radiative transfer in the disk atmosphere, the ray-tracing method to incorporate general relativity effects in light propagation, can be fitted (e.g. Hubeny et al. 2000; Loska et al. 2004; Sadowski et al. 2009; Czerny et al. 2011; Laor & Davis 2011; Czerny et al. 2019). Generally, the RM and the single-epoch virial BH mass method are inadequate for BH mass estimation in WLQs, due to weakness of emission-lines in these objects.

This paper is organized as follows. Section 2 consists of the description of data selection and reduction. Section 3 explains procedures used to fit models of accretion disk to observations. Section 4 presents our results. Discussions and conclusion are presented in Sections 5 and 6. In this work we compute luminosity distances using the standard cosmological model ($H_0 = 70 \text{ km s}^{-1} \text{ Mpc}^{-1}$, $\Omega_\Lambda = 0.7$, and $\Omega_M = 0.3$ (Spergel et al. 2007).

2. SAMPLE SELECTION AND DATA PREPARATION

2.1. Sample selection

The sample contains 10 WLQs, which positions cover a wide range of redshift from 0.2 to 3.5 (see Tab. 1). Four objects, namely SDSS J083650.86+142539.0 (thereafter J0836), SDSS J141141.96+140233.9 (J1411), SDSS J141730.92+073320.7 (J1417), and SDSS J144741.76-020339.1 (J1447) were analysed by Shen et al. (2011a); Plotkin et al. (2015). Three next sources – SDSS J114153.34+021924.3 (J1141) and SDSS J123743.08+630144.9 (J1237) were studied by

Diamond-Stanic et al. (2009), and SDSS J094533.98+100950.1 (J0945) by Hryniewicz et al. (2010). The quasar SDSS J152156.48+520238.5 (J1521) was inspected by Just et al. (2007); Wu et al. (2011). The number of objects in the sample from the SDSS campaign (Abazajian et al. 2009) has been increased by two next WLQs: PG 1407+265 and PHL 1811. The first object is the first observed WLQ in history and intensively examined by McDowell et al. (1995). PHL 1811 is the low redshift source classified also as NLS1 galaxy (Leighly et al. 2007a,b).

2.2. Observed data

Photometric points of WLQs at visible wavelengths are collected based on the Sloan Digital Sky Survey (SDSS) optical catalog Data Release 7. It contains the u, g, r, i, and z photometry (Abazajian et al. 2009). In the case of PHL 1811, we based on measurements of fluxes in B and R colors, and performed by the Dupont 100" telescope at Las Campanas Observatory (LCO) (Prochaska et al. 2011). The flux at U band was observed by the UVOT telescope on-board the *Swift* satellite (Page et al. 2014). Near-infrared photometry in the W1-W4 bands are taken from the Wide-field Infrared Survey Explorer (WISE) Preliminary Data Release (Wright et al. 2010; Wu et al. 2012b). Those data were supplied by photometry in the J, H, K_s colors obtained from the Extended Source Catalog of the Two Micron All Sky Survey (2MASS) (Skrutskie et al. 2006). Crucial points for the project are those detected in near- and far-ultraviolet (NUV, FUV, respectively) wavelengths. They are provided by the Galax Catalog Data Release 6 (Bianchi et al. 2017).

Additionally, we use the spectra observed by SDSS, to check photometric data positions in regards to the spectrum. In the case of PHL 1811 and PG 1407+265 the spectra are taken from Leighly et al. (2007a) and McDowell et al. (1995), respectively. A basic observational properties of the WLQs sample and sources of their photometry points are listed in Tab. 1.

To check if our disk fitting method works with respect to WLQs correctly, we are running a sample method of normal type 1 quasars. For this purpose, we select the sample of objects taken from the Large Bright Quasar Survey (LBQS) (Hewett et al. 1995, 2001). It is one of the largest published spectroscopic surveys of optically selected quasars at bright apparent magnitudes. It contains data, including positions and spectra of 1067 quasars. Additionally, Vestergaard & Osmer (2009) give black hole masses and Eddington accretion rates estimates of 978 LBQS (see their Table 2). The disk fitting method gives results that we can trust as long as the

Table 1. Sample of Weak Emission-Line Quasars and the sources of their photometry points

Name	RA	Dec	z_{spec}	A_V	Photometry data
	(deg.)	(deg.)		(mag.)	
(1)	(2)	(3)	(4)	(5)	(6)
SDSS J083650.86+142539.0	129.211935	+14.427527	1.749	0.129	WISE (W1,W2,W3), SDSS (u,g,r,i,z), Galex (NUV)
SDSS J094533.98+100950.1	146.391610	+10.163912	1.683	0.062	2MASS (J,H,K _s), SDSS (u,g,r,i,z), Galex (NUV,FUV)
SDSS J114153.34+021924.3	175.472251	+02.323508	3.55	0.065	WISE (W1,W2,W3,W4), SDSS (u,g,r,i,z)
SDSS J123743.08+630144.9	189.429435	+63.029141	3.49	0.032	WISE (W1,W2,W3,W4), SDSS (u,g,r,i,z)
SDSS J141141.96+140233.9	212.924908	+14.042742	1.754	0.064	WISE (W1,W2,W3,W4), SDSS (u,g,r,i,z), Galex (NUV,FUV)
SDSS J141730.92+073320.7	214.378855	+07.555744	1.716	0.084	WISE (W1,W2,W3,W4), SDSS (u,g,r,i,z), Galex (NUV,FUV)
SDSS J144741.76-020339.1	221.924048	-02.060986	1.430	0.163	WISE (W1,W2), SDSS (u,g,r,i,z), Galex (NUV,FUV))
SDSS J152156.48+520238.5	230.485324	+52.044062	2.238	0.052	WISE (W1,W2,W3,W4), 2MASS (J,H,K _s), SDSS (u,g,r,i,z)
PHL 1811	328.756274	-09.373407	0.192	0.133	WISE (W1,W2,W3,W4), 2MASS (J,H,K _s), LCO (B,R), Swift (U), Galex (NUV,FUV)
PG1407+265	212.349634	+26.305865	0.940	0.043	WISE (W1,W2,W3), 2MASS (J,H,K _s), SDSS (u,g,r,i,z)

NOTE— The coordinates (Col. 2 and 3), spectral redshift (Col. 4), and foreground Galactic extinction measured at the V color (Col. 5) are taken from NED. The column (6) contains references to the names of the relevant catalogs and photometric points.

bend point in SED and the spectrum in the ultraviolet are visible. For this reason, we have chosen 27 quasars with the presence of a well visible big blue bump. The sample of the normal quasars are observed at redshifts between 0.254 and 3.36. Their supermassive black holes masses are in the range 8.09–10.18 [in $\log M_{BH} (M_\odot)$, Fig. 1], and luminosities, $\log L_{bol} (\text{erg s}^{-1}) = 45.25$ –47.89. Photometric points of selected quasars come from the same catalogs mentioned earlier.

2.3. Dereddening

The observational data requires corrections, because they are contaminated either by internal or external effects such as a dust in our Galaxy, an influence of the intergalactic medium, starlight from the host galaxy, a dusty torus in the AGN. Firstly, the Spectral Energy Distribution (SED) of all objects are corrected for Galactic reddening with an extinction law. This extinction curve is usually parameterized in terms of the V-band extinction, A_V , and a measure of the relative extinction between B and V-band: $R_V = A_V/E(B-V)$. The value of R_V varies from 2.6 to 5.5 in the measurements of the diffuse interstellar medium with a mean value of 3.1 (Cardelli et al. 1989; Fitzpatrick 1999). A_V values are taken from NED¹ based on the dust map created by Schlegel et al. (1998). Cardelli et al. (1989) extinction

curve has cutoff at 1250 Å and some photometric points we use go back to shorter wavelengths. Nevertheless, the extinction law examined in the range of 900–1200 Å seems to follow the Cardelli et al. law (Hutchings & Giasson 2001). In this way, we extrapolate the curve down to 900 Å for our FUV photometric points by using the same formula.

2.4. UV and SDSS photometric points' correction

In the case of high- z quasars, the UV fluxes are very sensitive to photoelectric absorption in the intergalactic medium (IGM). We do not know an attenuation of the flux by the IGM along each line of sight. Therefore, following Castignani et al. (2013), we have used the effective optical depth $\tau_{eff}(\nu, z)$, which are averaged over all possible directions. Based on the values collected in Castignani's et al. Table 1, we correct the observed intensity: $I_{\nu,em} = I_{\nu,obs} \exp(\tau_{eff}(\nu, z))$. Thus, we recalculate the fluxes in the Galex FUV and NUV, the Swift U band, and the SDSS u, g filters. The effective optical depth in the three other SDSS filters (i.e. r, i, and z) vanishes for the redshift range considered here.

2.5. Starlight

A contribution to the SED from stars in the QSO host galaxy is likely to be negligible (Shen et al. 2011b; Collinson et al. 2015). Nevertheless, we would like to check its contribution and we determine a level of the starlight for each of objects individually. Follow-

¹ The NASA/IPAC Extragalactic Database (NED): ned.ipac.caltech.edu

Table 2. Fitted temperature of torus

Name	Temperature [K]
J0836	450, 1400
J0945	-
J1141	450, 970
J1237	430, 970
J1411	410, 970
J1417	430, 970
J1447	410, 1250
J1521	750
PHL 1811	450, 1100
PG 1407	650, 1240

ing Collinson et al., we use a 5 Gyr-old elliptical galaxy template² as the stars contamination to the fluxes. We estimate the level of the starlight using the $M_{\text{BH}}-L_{\text{bulge}}$ relation (DeGraf et al. 2015), where L_{bulge} is the bulge luminosity in the V-band (cyan line, in Fig. 2). M_{BH} are the BH masses in WLQs collected from literature (see Col. 7 in Tab. 4). We noticed that starlight has bigger contribution to WISE points than to the optical/UV data and adding contamination of the starlight to those data helps us refine the fitting procedure.

2.6. Torus contamination

Together with accretion disk emission, we fit one or two single-temperature blackbody (BB) as a thermal emission of tori visible at IR data (see Fig. 2). The fitted temperatures are collected in Tab. 2. The mean values of them for the two BB components are 1110 K and 460 K, respectively. Those values are close to those referred as 'hot' and 'warm' BB components (1100-2200K vs. 300-700K) by Collinson et al. (2017). The temperatures of 'hot' component are also similar to those seen in WLQs (870 K < T < 1240 K; Diamond-Stanic et al. 2009).

3. METHOD

3.1. Model of an accretion disk

The primary goal of this work is to fit SED of quasars by the simple geometrically thin and optically thick accretion disk (AD) model described by Novikov & Thorne (NT) equations. In the simplest approach, the AD continuum can be illustrated by the Shakura & Sunyaev model, nevertheless this attitude does not include a non-zero spin. The solution to this problem has resulted in the NT equations that we use in our numerical code.

Table 3. Parameter values for the grid of the AD models

Parameter	Δ	min-max values
$\log M_{\text{BH}}$	0.1	6–12
\dot{m}	0.01	0–1
a_*	0.1	0–0.9
i	15°	0°–75°

As the spin of the black hole increases, the innermost stable circular orbit (ISCO) decreases and the disk produces more high-energy radiation. The output continuum of the NT model is fully specified by four parameters, which we determine. These 4 parameters are: the black hole mass – M_{BH} , the mass accretion rate – \dot{M} , the dimensionless spin³ – a_* , and the inclination – i at which an observer looks at the AD. The mass of the black hole is expressed in units of mass of the Sun (M_{\odot}), and the accretion rate in the form of the Eddington rate, i.e. $\dot{m} = \dot{M}/\dot{M}_{\text{Edd}} \propto \dot{M}/M_{\text{BH}}$. We construct a grid of 366000 models of AD, for evenly spaced values of M_{BH} , \dot{m} , a_* , and i . The $\log M_{\text{BH}}$ range is from 6.0 to 12.0, the Eddington accretion rate covers the band 0–1, and the dimensionless spin $0 \leq a_* \leq 0.9$ with the step 0.1. The inclination is fixed for 6 values that cover a range from 0° to 75° with the step of 15° (see Tab. 3).

It is important to determine the radiative efficiency, η , in the SED fitting method. There are many approaches to estimate it. The $\eta \simeq 0.057$ computed for non-rotating BH. Shankar et al. (2009) suggest $\eta = 0.05 - 0.1$ in relation to AGNs. Observational constraints on growth of BHs made by Yu & Tremaine (2002) give us reasonable argument that η should be $\gtrsim 0.1$. Even more, Cao & Li (2008) proposed $\eta = 0.18$ for AGNs with BH masses above $10^9 M_{\odot}$. Performed analysis allows us to conclude that η should be in the range of 0.15 – 0.20. Those values are required to obtain the conformity of SMBH masses in LBQS if we use our SED fitting and single-epoch virial methods. Thus, we adopt the value of $\eta = 0.18$ in relation to both types of quasars – LBQS and WLQs.

We use a simple χ^2 procedure to find the best-fit model and evaluate the quality of the fit. It is based on directly matching the photometric points to the AD model. In our approach, we calculate $\chi^2 = \sum_{i=1}^n (O_i - E_i)^2 / \sigma_i$ for each quasar, where O_i and E_i are observed and modeled monochromatic luminosity L_{λ} which correspond to the i th photometric point, σ_i is the observed error, and n is the total number of observed data for the

² SWIRE Template Library: Polletta et al. (2007); www.iasf-milano.inaf.it/~polletta/templates/

³ $a_* = \frac{cJ}{GM^2}$

quasar. Satisfactory fits are defined as those showing reduced $\chi^2 \lesssim 5.5$.

In order to use information on yet determined black hole masses, accretion rates, and their errors in our WLQs sample we carry out a more sophisticated statistical analysis using the Bayesian method, which is the conditional distribution of the uncertain quantity given the data. The values of BH masses and accretion rates ($M_{\text{BH}}^{\text{lit}}$ and \dot{m}_{lit} , respectively) of 9 WLQs were collected by different authors (see Tab. 4, Col. 9) and those values for PG 1407 were determined by us (see Subsec. 3.1.1). Note, that both $M_{\text{BH}}^{\text{lit}}$ and \dot{m}_{lit} of WLQs are based on the $FWHM(\text{line})$ determination. Authors use equations with factors suitable for normal quasars which show strong lines and broad $FWHM$. However, this is not true for many WLQs. For this reason, both values $M_{\text{BH}}^{\text{lit}}$ and \dot{m}_{lit} could be calculated wrongly.

The Bayesian inference method requires the knowledge of the prior probability distribution $P(H|I)$, which represents our beliefs about a hypothesis H before some evidence, I , is taken into account. In our calculations H is j th model, $mod_j = mod(M_{\text{BH}j}, \dot{m}_j, a_{*j}, i_j)$, from among 366000 models we put in (note that both of the analyses i.e. χ^2 and the Bayesian, are based on the same set of constructed grid of the AD models). Any prior information about this j th model is I . In our case, the information I should be $M_{\text{BH}}^{\text{obs}}$, \dot{m}_{obs} , etc., which are observed. Nevertheless, we do not have those real parameters and therefore I is based on earlier calculated $M_{\text{BH}}^{\text{lit}}$, \dot{m}_{lit} and their errors. Assuming a Gaussian probability distribution for $M_{\text{BH}}^{\text{lit}}$ with standard deviations equal to σ_M , the prior can be written as $P(H|M_{\text{BH}}^{\text{lit}}) \propto \exp(-(M_{\text{BH}} - M_{\text{BH}}^{\text{lit}})^2/2\sigma_M^2)$. The prior probability related to \dot{m} takes a similar Gaussian form. We do not have a prior knowledge on either BH spin and inclination. We assume delta function probability distribution for both parameters.

For each j th model, we also derive its likelihood function $\mathcal{L}(mod_j) \propto \exp(-\chi^2/2) = P(D|mod_j, I)$, where D is the set of photometric points measured for each WLQ quasar. Note, that there is no free parameters.

Finally, the posterior probability is determined for each model, as the product of the likelihood and the priors on M_{BH} and \dot{m} (for details see Capellupo et al. 2015, Appendix A). It is given by:

$$P(H|D, I) = N \times \exp\left(\frac{-\chi^2}{2}\right) \times \exp\left(-\frac{(M_{\text{BH}} - M_{\text{BH}}^{\text{lit}})^2}{2\sigma_M^2}\right) \times \exp\left(-\frac{(\dot{m} - \dot{m}_{\text{lit}})^2}{2\sigma_{\dot{m}}^2}\right) \quad (2)$$

where N is the normalization constant.

The Bayesian analysis identifies a model which has the highest probability of explaining the observed SED assuming knowledge of BH mass and accretion rate. We find that the number of sources with satisfactory fit are the same and have high probability when we use the χ^2 and Bayes' theorem. The results for model with the highest posterior probability are shown in Tab. 6. Finally, we take the masses M_{BH} calculated from the χ^2 evaluation for further analysis.

3.1.1. BH mass and accretion rate determination in PG 1407, errors estimation for Bayesian analysis

There is a lack of the SMBH mass determination in the PG 1407 quasar. We estimate it based on the equation (7.27) from Netzer (2013), which states $M_{\text{BH}} \propto (\nu L_{\nu}(5100\text{\AA}))^{0.65} \times FWHM(H\beta)^2$. The level of continuum at 5100Å in PG 1407 is $\nu L_{\nu} = 3.16 \times 10^{46} \text{ erg s}^{-1}$ (McDowell et al. 1995). Unfortunately, the $H\beta$ emission-line is almost undetectably weak (McDowell et al. 1995). Firstly, we estimate $FWHM$ of Mg II line as follows. Using the Fe II template taken from Vestergaard & Wilkes (2001) we subtract contribution of the Fe II pseudo-continuum from magnesium line in the spectrum and we fit a Gauss function to it. The $FWHM(\text{Mg II})$ calculated in this way is equal to $4300_{-530}^{+1400} \text{ km s}^{-1}$. Next, we convert the width of magnesium to appropriate hydrogen based on the equation (6) by Wang et al. (2009): $\log(FWHM(\text{Mg II})) \propto 0.81 \times \log(FWHM(H\beta))$. Thus, $FWHM(H\beta) = 5400_{-810}^{+2240} \text{ km s}^{-1}$. Finally, the calculated BH mass is $M_{\text{BH}}^{H\beta} = (2.62_{-0.73}^{+2.61}) \times 10^9 M_{\odot}$ and we take this value as $M_{\text{BH}}^{\text{lit}}$ (Tab. 4). Additionally, we calculate BH mass based on Mg II line following the similar procedure. We use equation (7.28) from Netzer (2013) and get $M_{\text{BH}}^{\text{Mg(II)}} = (3.69_{-0.85}^{+2.79}) \times 10^9 M_{\odot}$.

The accretion rate in PG 1407 is calculated using relationship $L_{\text{Bol}}/L_{\text{Edd}} \propto f(L) \times (L_{5100\text{\AA}})^{0.5} \times (FWHM(H\beta))^{-2}$ (see equation 2 in Plotkin et al. 2015), where $f(L)$ is the luminosity-dependent bolometric correction and equals to 5.7 (Shemmer et al. 2010). Eventually, $\dot{m}_{\text{lit}} = 0.45$ based on calculated $FWHM(H\beta)$ and luminosity at 5100Å in PG 1407.

For Bayesian analysis we need to determine the errors of the accretion rates of those WLQs for which, the literature does not provide them. We use mentioned equation (2) (see Plotkin et al. 2015), upper and lower limits of $FWHM(H\beta)$ and $L_{5100\text{\AA}}$. Errors of \dot{m}_{lit} are listed in Tab. 4.

4. RESULTS

For initial analysis, we use 27 quasars from the LBQS survey (see Sec. 2). Fig. 1 shows us a comparison of the

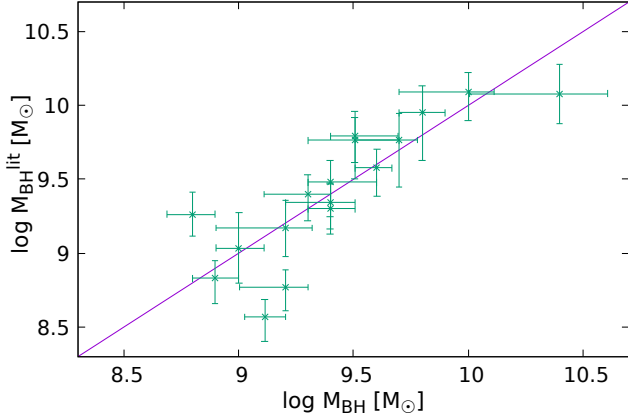


Figure 1. Comparison of LBQS masses (on the y-axis) with M_{BH} from our model (on the x-axis). Violet solid line is identity 1:1 line.

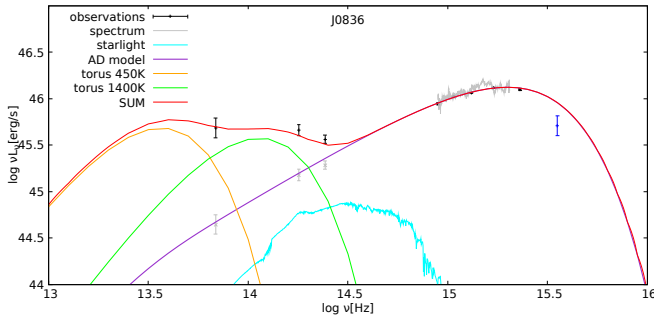


Figure 2. The best fit of WLQ SDSS J083650.86+142539.0. Summary of all components. Black points with errors show photometry data, grey line represents spectrum. Violet line shows contribution of the AD model. Tori with temperature 450K and 1400K, respectively, are displayed by orange and green lines. Cyan line points the level of starlight out. Sum of the components thus the best fit is shown by red line.

supermassive black hole masses determined by Vestergaard & Osmer (2009), $M_{\text{BH}}^{\text{lit}}$ (on the y-axis), to those obtained by us, M_{BH} (on the x-axis). Both masses are given in mass units of the Sun. Violet solid line is a 1:1 identity line. Vestergaard & Osmer (2009) used the black hole mass determination based on their formula (1), which is proportional to $FWHM(\text{line})$ and luminosity νL_ν . We would like to note that we use the same grid of 366000 models (see Sec. 3) to obtain M_{BH} . Compliance of masses and relatively small distribution of errors means that the continuum fitting method applies to quasars.

Our sample of weak emission-line quasars contains 10 objects. Fig. 2 shows in detail how the fitting procedure works. Different lines show the individual components: accretion disk, tori, starlight level. Solid red line shows sum of those components. The same approach is used in

the rest of 9 WLQs. Fig. 3 presents the best fits of disk continua that match the quasars SED. On the x-axis is the logarithmic value of frequency in Hertz, while on the y-axis is the logarithmic value of νL_ν in erg s^{-1} . The accretion disk continuum is marked with a solid purple line, the photometric data are shown by black crosses and blue points with errors. The blue points observed in UV bandpass of 5 WLQs (J0836, J1141, J1411, J1417, and J1447) and in optical range (J0836) could suggest an absorption seen in some quasars (e.g. KVRQ 1500-0031 Heintz et al. 2018, SDSS J080248.18+551328.9 Ji et al. 2015; Liu et al. 2015). The absorption are caused by intrinsic gas in the host galaxy and/or bigger influence of the assumed UV photoelectric absorption. Blue points are outliers and for this reason we model the best fits in both cases: taking into consideration all points with and without outliers (χ^2 values in parenthesis of Tab. 4).

Our results are collected in Tab. 4. The black hole masses, accretion rates, spins, inclinations of each WLQs, and χ^2 values are in Columns (1)-(6). Columns (7) and (8) contain the literature values of the black hole masses and the accretion rates, respectively. Column (9) contains references to the above values, as appropriate. Degeneration of solutions due to the spin parameter takes place. Two groups of the best fit for zero and non-zero spin are difficult to distinct. Thus, we also perform additional fit with the fixed a_* equals 0 (Tab. 5). In this approach, the photometric points without outliers are taken into account (only black points in Fig. 3).

Additionally, the black hole masses determined from the Bayesian analysis are presented in Tab. 6. No significant differences in black hole masses calculated from both the χ^2 and the Bayesian analysis are indicated. It suggests that the determined global parameters are correct and describe the overall SED shape of these objects. We take the values from Tab. 4 for further analysis.

Fig. 4 shows the mass distribution of black holes. Identity 1:1 line is marked as solid purple line. The presented mass comparison suggests that literature determinations of black hole masses, $M_{\text{BH}}^{\text{lit}}$, based on $FWHM(H\beta)$ are generally underestimated. We also determine the difference between $M_{\text{BH}}^{\text{lit}}$ and M_{BH} values. The γ factor is calculated ($\gamma = M_{\text{BH}}/M_{\text{BH}}^{\text{lit}}$). In Fig. 5 we present the relationship between the logarithmic value of $FWHM(H\beta)$ in km s^{-1} (see Tab. 7) and the logarithmic value of the γ factor. The green solid line shows the best fit between those variables. The fit is made using the nonlinear least-squares (NLLS) Marquardt-Levenberg algorithm which takes into account errors in

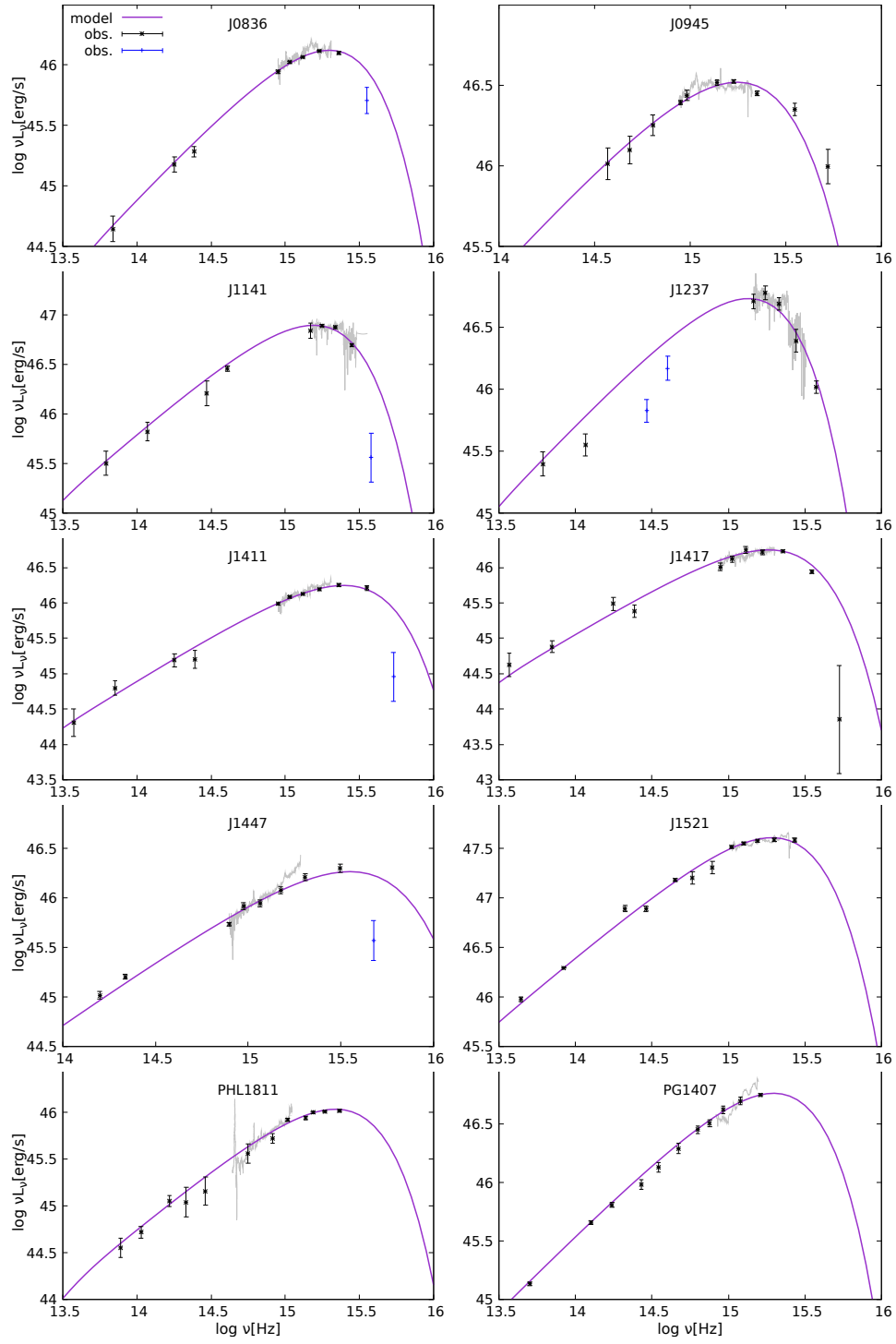


Figure 3. The best fit of SED to photometric points of 10 WLQs. Black crosses and blue with errors show corrected observational data, grey line – spectra. Violet solid line represents the theoretical curve of the AD continuum model.

Table 4. The best fit parameters

Name	M_{BH}	\dot{m}	a_*	i	$\chi^2/\text{d.o.f}$	$M_{\text{BH}}^{\text{lit}}$	$\dot{m}_{\text{lit.}}$	ref.
(1)	(2)	(3)	(4)	(5)	(6)	(7)	(8)	(9)
J0836	$(1.30^{+5.00}_{-0.30}) \times 10^9$	$0.38^{+0.28}_{-0.25}$	$0.00^{+0.30}_{-0.00}$	$0.26^{+0.52}_{-0.26}$	2.48 (1.91)	$(3.89^{+13.11}_{-1.75}) \times 10^8$	$0.87^{+1.36}_{-0.65}$	1/1
J0945	$(2.00^{+4.30}_{-0.50}) \times 10^9$	$0.47^{+0.19}_{-0.16}$	$0.00^{+0.30}_{-0.00}$	0.52 ± 0.26	3.73	$(1.12^{+0.43}_{-0.19}) \times 10^9$	0.51 ± 0.15	1/1
J0945						$(3.08 \pm 0.27) \times 10^9 \dagger$		2
J1141	$(6.30^{+13.70}_{-1.30}) \times 10^9$	$0.56^{+0.28}_{-0.36}$	$0.10^{+0.40}_{-0.10}$	0.26 ± 0.26	4.58 (2.67)	$(3.16^{+1.41}_{-0.97}) \times 10^9$	$0.38^{+0.20}_{-0.10} *$	3/3
J1237	$(5.00^{+6.00}_{-1.80}) \times 10^9$	$0.30^{+0.29}_{-0.21}$	$0.10^{+0.60}_{-0.10}$	$0.26^{+0.52}_{-0.26}$	6.64 (3.93)	$(2.00^{+1.39}_{-0.65}) \times 10^9$	$0.40^{+0.21}_{-0.16} *$	3/3
J1411	$(2.50^{+0.70}_{-1.20}) \times 10^9$	$0.31^{+0.44}_{-0.08}$	$0.80^{+0.10}_{-0.40}$	$0.26^{+0.52}_{-0.26}$	5.58 (1.25)	$(5.25^{+3.87}_{-2.23}) \times 10^8$	$0.34^{+0.42}_{-0.17}$	1/1
J1417	$(3.20^{+0.70}_{-1.90}) \times 10^9$	$0.54^{+0.19}_{-0.41}$	$0.20^{+0.30}_{-0.10}$	$0.00^{+0.52}_{-0.00}$	2.88	$(3.55^{+3.53}_{-2.15}) \times 10^8$	0.92 ± 0.50	1/1
J1447	$(1.30^{+1.20}_{-6.30}) \times 10^9$	$0.35^{+0.41}_{-0.07}$	0.80 ± 0.10	0.26 ± 0.26	5.37 (4.41)	$(1.12^{+2.51}_{-1.25}) \times 10^8$	$1.30^{+0.17}_{-0.78}$	1/1
J1521	$(2.00^{+0.50}_{-5.70}) \times 10^{10}$	$0.48^{+0.19}_{-0.35}$	$0.80^{+0.10}_{-0.20}$	$0.52^{+0.26}_{-0.52}$	3.68	$(6.20^{+1.73}_{-1.51}) \times 10^9$	$0.81^{+0.27}_{-0.17} *$	4/4
PHL 1811	$(7.90^{+2.10}_{-3.90}) \times 10^8$	$0.34^{+0.50}_{-0.03}$	$0.00^{+0.10}_{-0.00}$	$0.00^{+0.26}_{-0.00}$	1.87	$(1.14^{+2.57}_{-2.57}) \times 10^8$	$1.30^{+0.03}_{-0.02} *$	5/5
PG 1407	$(7.90^{+5.10}_{-2.90}) \times 10^9$	$0.26^{+0.28}_{-0.09}$	$0.90^{+0.00}_{-0.10}$	0.78 ± 0.26	1.42	$(2.62^{+2.61}_{-0.73}) \times 10^9$	$0.45^{+0.17}_{-0.23} *$	a/a
PG 1407						$(3.69^{+2.79}_{-0.85}) \times 10^9 \dagger$		a

NOTE— Black hole masses, Eddington accretion rates, spins, and fitted inclinations are in Col. (2)-(5), respectively. Col. (6) contains the normalized χ^2 values in two cases: numbers without parenthesis – all photometric points are taken into account, numbers in parenthesis – data with removed outliers (only black points in Fig. 3) are considered. The values in Col. (2)-(5) refer to the case where all points are fitted. The values of the parameters in the absence of outliers are the same as before within the errors. Black hole masses and accretion rates taken from literature are in Col.(7)-(8). They are based on $FWHM(\text{H}\beta)$ measurements (values without \dagger). \dagger – M_{BH} is based on Mg II line. M_{BH} and $M_{\text{BH,lit.}}$ are in units of M_{\odot} . * – errors of $\dot{m}_{\text{lit.}}$ are estimated by us. Numbers refer to articles: 1) Plotkin et al. (2015), 2) Hryniewicz et al. (2010), 3) Shemmer et al. (2010), 4) Wu et al. (2011), 5) Leighly et al. (2007b), 6) McDowell et al. (1995), a) this work.

Table 5. The Schwarzschild black hole solutions ($a_*=0$)

Name	M_{BH}	\dot{m}	i	$\chi^2/\text{d.o.f}$
J0836	$(1.30^{+5.00}_{-0.30}) \times 10^9$	$0.38^{+0.28}_{-0.25}$	$0.26^{+0.52}_{-0.26}$	(1.91)
J0945	$(2.00^{+4.30}_{-0.50}) \times 10^9$	$0.47^{+0.19}_{-0.16}$	0.52 ± 0.26	(3.73)
J1141	$(7.90^{+2.10}_{-2.90}) \times 10^9$	$0.84^{+0.03}_{-0.28}$	$1.30^{+0.00}_{-0.52}$	(4.11)
J1237	$(4.00^{+2.30}_{-0.80}) \times 10^9$	$0.30^{+0.06}_{-0.29}$	$0.00^{+0.26}_{-0.00}$	(4.54)
J1411	$(7.90^{+3.40}_{-1.60}) \times 10^9$	$0.50^{+0.03}_{-0.11}$	$0.00^{+0.26}_{-0.00}$	(1.43)
J1417	$(2.50^{+0.70}_{-0.50}) \times 10^9$	$0.66^{+0.19}_{-0.22}$	$1.30^{+0.00}_{-0.26}$	(1.98)
J1447	$(5.00^{+2.90}_{-1.00}) \times 10^9$	$0.49^{+0.20}_{-0.05}$	$0.78^{+0.52}_{-0.26}$	(4.96)
J1521	$(1.30^{+0.70}_{-3.40}) \times 10^{10}$	$0.86^{+0.11}_{-0.63}$	$1.30^{+0.00}_{-0.52}$	(3.99)
PHL 1811	$(7.90^{+2.10}_{-3.90}) \times 10^8$	$0.34^{+0.50}_{-0.03}$	$0.00^{+0.26}_{-0.00}$	(1.87)
PG 1407	$(2.50^{+0.70}_{-0.50}) \times 10^9$	$0.85^{+0.06}_{-0.19}$	0.78 ± 0.26	(0.93)

NOTE— The normalized χ^2 values in parenthesis means the data with removed outliers (only black points in Fig. 3) are considered.

both x and y directions. The relationship is:

$$\log \gamma = (-1.338 \pm 0.366) \times \log \left(\frac{FWHM(H\beta)}{10^3 \text{ km s}^{-1}} \right) + (1.294 \pm 0.234) \quad (3)$$

For a better assessment of our calculations, we have determined the Spearman coefficient, which is $r_s = -0.806$ and the linear correlation coefficient, $r = -0.82$. It can be seen that three of the ten objects (J0945, J1141, and J1237) are close to 1:1 line and the γ factor is $\lesssim 2.5$. Masses of three other sources (PHL 1811, J1417, J1447) should be multiplied by $\gamma > 7$. The mean γ factor is 4.7, and median is 3.3. The dashed blue line in Fig. 5 represents the best fit obtained by Mejía-Restrepo et al. (2018a). They used a sample of 37 Type I AGNs, which lie in the range of redshifts ~ 1.5 . Eq. (3) allows us to correct the black hole masses, $M_{\text{BH}}^{\text{lit}}$, determined so far and based on $FWHM$ values of $H\beta$ line.

5. DISCUSSION

The virial factor (f in Eq. 1) is often assumed to be constant with values of 0.6-1.8 (e.g. Peterson 2004; Onken et al. 2004; Nikolaïjuk et al. 2006), where 0.75 corresponds to a spherical geometry of the BLR. Generally, f depends on non-virial velocity components such as winds, the relative thickness (H/R_{BLR}) of the Keplerian BLR orbital plane, the line-of-sight inclination angle (i) of this plane, the radiation pressure (Wills & Browne 1986; Gaskell 2009; Denney et al. 2009, 2010; Shen & Ho 2014; Runnoe et al. 2014) and it should be a function of those phenomenons. The analysis carried out by Mejía-Restrepo et al. (2018a) indicates a low influence of radiation pressure on the f factor, however

Table 6. The BH masses from the Bayesian analysis

Name	$M_{\text{BH}}^{\text{Bay}} [\text{M}_{\odot}]$
J0836	$(2.00^{+4.30}_{-1.00}) \times 10^9$
J0945	$(3.20^{+3.10}_{-1.20}) \times 10^9$
J1141	$(7.90^{+4.10}_{-2.90}) \times 10^9$
J1237	$(6.30^{+3.70}_{-1.30}) \times 10^9$
J1411	$(1.30^{+1.90}_{-1.30}) \times 10^9$
J1417	$(2.50^{+2.50}_{-1.20}) \times 10^9$
J1447	$(1.00^{+1.50}_{-6.00}) \times 10^9$
J1521	$(1.30^{+1.20}_{-5.00}) \times 10^{10}$
PHL 1811	$(7.90^{+3.10}_{-3.90}) \times 10^8$
PG 1407	$(7.90^{+3.40}_{-2.90}) \times 10^9$

Table 7. The Full Width at Half Maximum of $H\beta$ emission-line and the γ factor

Name	$FWHM(H\beta) [\text{km s}^{-1}]$	$\log \gamma$	ref.
J0836	2880^{+1877}_{-1069}	$0.52^{+0.18}_{-0.31}$	1
J0945	4278 ± 598	$0.25^{+0.11}_{-0.16}$	1
J1141	5900^{+1000}_{-1100}	$0.30^{+0.14}_{-0.20}$	2
J1237	5200^{+1500}_{-1000}	$0.40^{+0.17}_{-0.29}$	2
J1411	3966 ± 1256	$0.68^{+0.22}_{-0.44}$	1
J1417	2784 ± 759	$0.96^{+0.27}_{-0.82}$	1
J1447	1923^{+933}_{-164}	$1.06^{+0.18}_{-0.32}$	1
J1521	5750 ± 750 *	$0.51^{+0.36}_{-0.44}$	3
PHL 1811	1943 ± 19	$0.84^{+0.3}_{-0.52}$	4
PG 1407	5400^{+2240}_{-810} ‡	$0.47^{+0.17}_{-0.26}$	a

NOTE— $\gamma = M_{\text{BH}}/M_{\text{BH}}^{\text{lit}}$. * – errors are estimated by us. ‡ $H\beta$ is weak and almost not visible, its $FWHM$ is estimated based on $FWHM$ (Mg II). Numbers refer to $FWHM$ sources: 1) Plotkin et al. (2015), 2) Shemmer et al. (2010), 3) Wu et al. (2011), 4) Leighly et al. (2007b), a) this work.

this mechanism cannot be excluded. Whether or not we skip the radiation pressure influence, the line-of sight inclination of gas in a planar distribution of the BLR plays important role in black hole mass calculations. Unfortunately, the nature of the velocity component responsible for the thickness of the BLR and thus its geometry is unclear (e.g. Done & Krolik 1996; Collin et al. 2006; Czerny et al. 2016; for recent review see Czerny 2019).

Our results support those got by Mejía-Restrepo et al. (2018a). They study 37 AGNs at redshifts ~ 1.5 . The authors indicate the dependency of the virial factor, on observed $FWHM$ of the broad emission-line (such as $H\beta$, Mg II, C IV) in the form of an anti-correlation. It implies that the BH mass estimations based on the reverberation or the single-epoch virial BH mass method

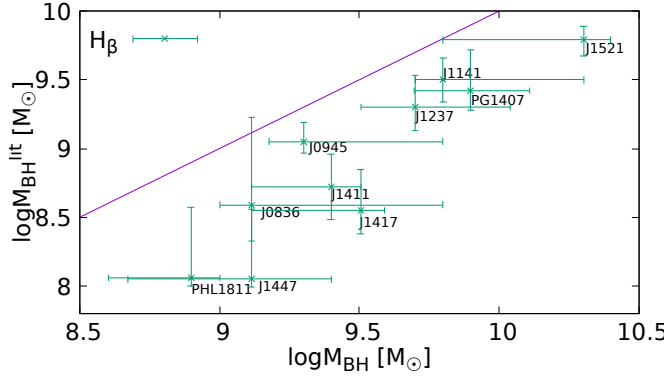


Figure 4. Comparison of SMBH masses ($M_{\text{BH}}^{\text{lit}}$) of WLQs based on $FWHM$ estimations with M_{BH} , that come from spectral fitting method. Violet solid line is identity 1:1 line. Green crosses represent $M_{\text{BH}}^{\text{lit}}$ calculated using $FWHM$ of $H\beta$.

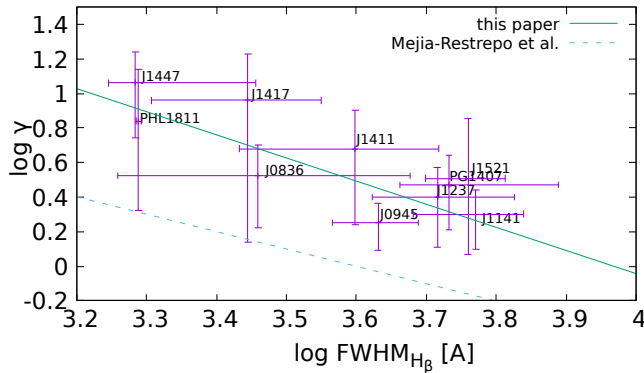


Figure 5. The γ factor ($= M_{\text{BH}}/M_{\text{BH}}^{\text{lit}}$) versus $FWHM(H\beta)$. The best fit (i.e. $\gamma \propto FWHM^{-1.34}$) is shown by green solid line. Points show data of 10 WLQs. The blue dash line represents the fit of the virial factor (i.e. $f \propto FWHM^{-1.17}$) to 37 AGNs made by Mejía-Restrepo et al. (2018a). In our case $\gamma = \text{const} \times f$ and the dash line is shifted down.

are systematically overestimated for AGN systems with larger $FWHM$ (e.g. $\gtrsim 4000 \text{ km s}^{-1}$ for $H\alpha$) and underestimated for systems with small $FWHM(H\alpha) \lesssim 4000 \text{ km s}^{-1}$. It is worth to note that the opposite rule applies to the Eddington accretion rates (because $\dot{m} \propto M_{\text{BH}}^{-1}$). We found a similar underestimation of $M_{\text{BH}}^{\text{lit}}$ values in the sample of WLQs (Fig. 5). SMBH masses of AGNs, which show $FWHM(H\beta) \gtrsim 5000 \text{ km s}^{-1}$ need to be multiplied by a small factor of 1.5-2.5 while the rest of them requires the larger factor up to 12. It means that the masses of about 50-60% of WLQs are underweight based on $FWHM(H\beta)$ values.

It can be seen in Fig. 4 that the correction of the SMBH masses based on $FWHM$ estimation is needed.

We modify $M_{\text{BH}}^{\text{lit}}$ (Equation 1 in Plotkin et al. 2015):

$$\frac{M_{\text{BH}}^{\text{lit}}}{10^6 M_{\odot}} = 5.05 \left(\frac{\nu L_{\nu}(5100)}{10^{44} \text{ erg s}^{-1}} \right)^{0.5} \left(\frac{FWHM(H\beta)}{10^3 \text{ km s}^{-1}} \right)^2 \quad (4)$$

using the definition of the γ factor ($M_{\text{BH}} = \gamma \times M_{\text{BH}}^{\text{lit}}$) and Eq. (3). The corrected formula for the SMBH masses in WLQs is:

$$\frac{M_{\text{BH}}}{10^7 M_{\odot}} = (9.94_{-4.13}^{+7.09}) \times \left(\frac{\nu L_{\nu}(5100)}{10^{44} \text{ erg s}^{-1}} \right)^{0.5} \times \left(\frac{FWHM(H\beta)}{10^3 \text{ km s}^{-1}} \right)^{0.66 \pm 0.37} \quad (5)$$

The weaker dependence on $FWHM(H\beta)$ can be realized when the BLR is elongated and parallel to the accretion disk. There is accumulated evidence in the literature favoring a disk-like geometry for the BLR (Wills & Browne 1986; Laor et al. 2006; Decarli et al. 2008; Pancoast et al. 2014; Shen & Ho 2014; Mejía-Restrepo et al. 2018b; Wang et al. 2019). On the other hand, the BLR may be also dominated by outflows, which are perpendicular to the line-of-sight. This scenario will favor a quasar reactivation idea. The outflow could rebuild the $H\beta$ region (Hryniewicz et al. 2010).

Systematic underestimation of $FWHM$ (and $M_{\text{BH}}^{\text{lit}}$) may also be caused by a strong influence of the Fe II pseudo-continuum in optics. Such phenomena is noticed by Plotkin et al. (2015) for their sample of WLQs, which have larger $R_{\text{opt,FeII}}$ and narrower $H\beta$ than most reverberation mapped quasars.

Mejía-Restrepo et al. (2018a) find that the dependence of M_{BH} on the observed $FWHM$ of the Balmer lines for AGNs is close to linear rather ($M_{\text{BH}} \propto FWHM(H\beta)^{0.82 \pm 0.11}$, when f is a function of the Full Width) than quadratic ($M_{\text{BH}} \propto FWHM^2$ with $f = \text{const}$). In our case, this relationship for WLQs is a bit weaker ($M_{\text{BH}} \propto FWHM(H\beta)^{0.66 \pm 0.37}$), but still compatible with the Mejía-Restrepo et al. result within 1σ error. A similar or even the same behavior of normal AGNs and WLQs suggests that both kind of sources have the same dim nature of the velocity component and similar geometry of the BLR.

The relationship between the widths of Mg II and $H\beta$ emission-lines is noticed in AGNs (see Shen et al. 2008; Wang et al. 2009). The estimation of BH masses based on those lines are consistent with each other. However, a bias between the C IV and Mg II mass estimation suggests that the C IV estimator is severely affected by an outflow (Baskin & Laor 2005; Trakhtenbrot & Netzer 2012; Kratzer & Richards 2015). The authors argue that using $H\beta$ or Mg II is better for BH mass estimation than C IV. Similar note is made by Shen et al., whose results

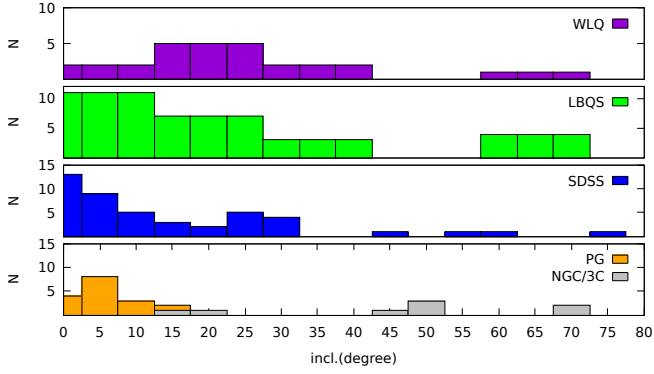


Figure 6. The distribution of inclinations in AGNs. Our sample of WLQs and LBQS quasars (the top panel and below). Blue histogram indicates SDSS quasars (Wildy et al. 2018). The lowest panel shows PG quasars (orange histogram), 3C and Seyfert 1 galaxies (grey color). The data come from Bian & Zhao (2002).

are based on 58 643 quasars from the SDSS catalog and who claim that the bias may be too large for individual objects using CIV estimator, but it is still consistent with Mg II and H β in the mean. On the other hand, Wang et al. (2009) have found that $FWHM(\text{Mg II})$ is systematically smaller than $FWHM(\text{H}\beta)$ and the BH masses based on Mg II estimator show subtle deviations from those commonly used. Referring to WLQs, Plotkin et al. (2015) suggest that using Mg II line could cause bias to the mass measurements due to the big contribution of the Fe II pseudo-continuum. Thus, in this work, we base the estimations of BH masses on $FWHM(\text{H}\beta)$ by trying to avoid C IV and Mg II.

In our paper we fix the value of the radiative efficiency $\eta = 0.18$. However, we would like to check its influence on the results. We again perform simulations and compare values of the best fits of BH masses and accretion rates in two cases, when $\eta = 0.18$ and $\eta = 0.36$. The accretion rates are 40-70% higher and the BH masses are on average 20-30 % less massive for higher η (for the first order approximation we have $M_{\text{BH}}^2 \dot{m} / \eta \simeq \text{const}$). Please note that such a decline in BH masses cannot explain underestimation of $M_{\text{BH}}^{\text{lit}}$ and the choice of solutions with $\eta \approx 0.18$ increases the χ^2 .

The agreement for LBQS and discrepancy for WLQ quasars between their virial and the SED masses may suggest that $FWHM$ is a biased indicator of the virial velocity, due to the inclination of the emission region of the H β line. The BLR in WLQs could be less face-on than those in LBQS and other quasars. We compare inclinations of WLQs and LBQS quasars in our sample with those derived from SDSS quasars (Wildy et al. 2018), PG quasars and Seyfert 1 galaxies (Bian & Zhao

2002). Generally, the main inclinations in LBQS are located at range 0-15 $^\circ$, whereas WLQs are shifted toward higher values with the main peak at 15-30 $^\circ$ (Fig. 6). We point out the same average inclination values in SDSS and LBQS quasars. It is worth to mention that fitted errors are significant. Thus, inclinations may be the same in all quasars. According to Collin & Kawaguchi (2004) (see their equation 11 and figure 8), bigger inclination in WLQs (e.g. $i_{\text{LBQS}} = 5^\circ \rightarrow i_{\text{WLQ}} = 20^\circ$) together with the assumption of the flat BLR geometry ($H/R_{\text{BLR}} \lesssim 0.3$) cause underestimation of $FWHM$ by a factor $\gtrsim 2.5$. If we assume that the widths with values in the order of 2000 km s $^{-1}$ are produced in the disk-like geometry, then BH masses should be heavier by 6-10 times. It is comparable with our analysis. Higher widths, like those in LBQS quasars, could be formed in the BLR with spherical geometry. In this case the calculated BH masses do not require a correction. It seems that the flatness of the BLR in the weak emission-line quasars plays a more important role than the inclination.

6. CONCLUSION

In this work we have studied the accretion disk continua of 10 WLQs. The SMBH masses of those objects are estimated previously based on the single-epoch virial BH mass method ($M_{\text{BH}}^{\text{lit}}$). We create grid of 366000 models using the Novikov-Thorne formulas. We adopt four parameters (M_{BH} , \dot{m} , spin of BH and the line-to-sight inclination) to describe the observed SED and compare obtained BH masses with those got from the literature.

Our main findings are:

1. Using the Novikov-Thorne model, we can describe very well the SED of WLQs.
2. The SMBH masses of WLQs, which are estimated based on $FWHM(\text{H}\beta)$, are underestimated. On average, the masses are undervalued by 4-5 times. The median of this correction factor is 3.3.
3. We propose the formula to estimate M_{BH} in WLQs based on their observed $FWHM(\text{H}\beta)$ and luminosities at 5100Å (Eq. 5). Our results suggest that selected WLQs have the accretion rates in the range ~ 0.3 -0.6.
4. We support Mejía-Restrepo et al. result and confirm that the virial factor, f , depends on $FWHM$. In this paper it $\propto FWHM(\text{H}\beta)^{-1.34 \pm 0.37}$. The BLR is a non-spherical region.
5. We suggest that WLQs are normal quasars in a reactivation stage, in which the BLR region has the disk-like geometry.

ACKNOWLEDGEMENTS

We would like to thank the anonymous referee for useful comments that improved the clarity of the paper. We also thank to Bożena Czerny, Ari Laor and Samuele Campitiello for helpful feedback and discussions. The authors acknowledge support from the (Polish) National Science Center Grant No. 2016/22/M/ST9/00583. We would like to thanks databases: The Sloan Digital

Sky Survey (SDSS), the Two Micron All Sky Survey (2MASS), Galaxy Evolution Explorer (GALEX), the Wide-field Infrared Survey Explorer (WISE) and VizieR service. This research has made use of the NASA/IPAC Extragalactic Database (NED), which is operated by the Jet Propulsion Laboratory, Caltech, under contract with the NASA.

REFERENCES

- Abazajian, K. N., Adelman-McCarthy, J. K., Agüeros, M. A., et al. 2009, *ApJS*, 182, 543
- Bañados, E., Venemans, B. P., Morganson, E., et al. 2014, *AJ*, 148, 14
- Baskin, A., & Laor, A. 2005, *MNRAS*, 356, 1029
- Bentz, M. C., & Manne-Nicholas, E. 2018, *ApJ*, 864, 146
- Bentz, M. C., Walsh, J. L., Barth, A. J., et al. 2009, *ApJ*, 705, 199
- Bian, W., & Zhao, Y. 2002, *A&A*, 395, 465
- Bianchi, L., Shiao, B., & Thilker, D. 2017, *ApJS*, 230, 24
- Blandford, R. D., & McKee, C. F. 1982, *ApJ*, 255, 419
- Cao, X., & Li, F. 2008, *MNRAS*, 390, 561
- Capellupo, D. M., Netzer, H., Lira, P., Trakhtenbrot, B., & Mejía-Restrepo, J. 2015, *MNRAS*, 446, 3427
- Cardelli, J. A., Clayton, G. C., & Mathis, J. S. 1989, *ApJ*, 345, 245
- Castignani, G., Haardt, F., Lapi, A., et al. 2013, *A&A*, 560, A28
- Collin, S., & Kawaguchi, T. 2004, *A&A*, 426, 797
- Collin, S., Kawaguchi, T., Peterson, B. M., & Vestergaard, M. 2006, *A&A*, 456, 75
- Collinson, J. S., Ward, M. J., Done, C., et al. 2015, *MNRAS*, 449, 2174
- Collinson, J. S., Ward, M. J., Landt, H., et al. 2017, *MNRAS*, 465, 358
- Czerny, B. 2019, *Open Astronomy*, 28, 200
- Czerny, B., Du, P., Wang, J.-M., & Karas, V. 2016, *ApJ*, 832, 15
- Czerny, B., Hryniewicz, K., Nikolaïuk, M., & Sądowski, A. 2011, *MNRAS*, 415, 2942
- Czerny, B., Wang, J.-M., Du, P., et al. 2019, *ApJ*, 870, 84
- Decarli, R., Dotti, M., Fontana, M., & Haardt, F. 2008, *MNRAS*, 386, L15
- DeGraf, C., Di Matteo, T., Treu, T., et al. 2015, *MNRAS*, 454, 913
- Denney, K. D., Peterson, B. M., Pogge, R. W., et al. 2009, *ApJL*, 704, L80
- . 2010, *ApJ*, 721, 715
- Diamond-Stanic, A. M., Fan, X., Brandt, W. N., et al. 2009, *ApJ*, 699, 782
- Done, C., & Krolik, J. H. 1996, *ApJ*, 463, 144
- Fan, X., Strauss, M. A., Gunn, J. E., et al. 1999, *ApJL*, 526, L57
- Fausnaugh, M. M., Grier, C. J., Bentz, M. C., et al. 2017, *ApJ*, 840, 97
- Fitzpatrick, E. L. 1999, *PASP*, 111, 63
- Gaskell, C. M. 2009, *NewAR*, 53, 140
- Heintz, K. E., Fynbo, J. P. U., Ledoux, C., et al. 2018, *A&A*, 615, A43
- Hewett, P. C., Foltz, C. B., & Chaffee, F. H. 1995, *AJ*, 109, 1498
- . 2001, *AJ*, 122, 518
- Hryniewicz, K., Czerny, B., Nikolaïuk, M., & Kuraskiewicz, J. 2010, *MNRAS*, 404, 2028
- Hubeny, I., Agol, E., Blaes, O., & Krolik, J. H. 2000, *ApJ*, 533, 710
- Hutchings, J. B., & Giasson, J. 2001, *PASP*, 113, 1205
- Ji, T., Zhou, H., Jiang, P., et al. 2015, *ApJ*, 800, 56
- Just, D. W., Brandt, W. N., Shemmer, O., et al. 2007, *ApJ*, 665, 1004
- Kaspi, S., Maoz, D., Netzer, H., et al. 2005, *ApJ*, 629, 61
- Kaspi, S., Smith, P. S., Netzer, H., et al. 2000, *ApJ*, 533, 631
- Kratzer, R. M., & Richards, G. T. 2015, *AJ*, 149, 61
- Laor, A., Barth, A. J., Ho, L. C., & Filippenko, A. V. 2006, *ApJ*, 636, 83
- Laor, A., & Davis, S. W. 2011, *MNRAS*, 417, 681
- Leighly, K. M., Halpern, J. P., Jenkins, E. B., & Casebeer, D. 2007a, *ApJS*, 173, 1
- Leighly, K. M., Halpern, J. P., Jenkins, E. B., et al. 2007b, *ApJ*, 663, 103
- Liu, W.-J., Zhou, H., Ji, T., et al. 2015, *ApJS*, 217, 11
- Liu, Y., & Zhang, S. N. 2011, *ApJL*, 728, L44
- Loska, Z., Czerny, B., & Szczerba, R. 2004, *MNRAS*, 355, 1080
- Luo, B., Brandt, W. N., Hall, P. B., et al. 2015, *ApJ*, 805, 122

- Marlar, A., Shemmer, O., Anderson, S. F., et al. 2018, *ApJ*, 865, 92
- McDowell, J. C., Canizares, C., Elvis, M., et al. 1995, *ApJ*, 450, 585
- Mejía-Restrepo, J. E., Lira, P., Netzer, H., Trakhtenbrot, B., & Capellupo, D. M. 2018a, *Nature Astronomy*, 2, 63
- . 2018b, *Nature Astronomy*, 2, 63
- Meusinger, H., & Balafkan, N. 2014, *A&A*, 568, A114
- Netzer, H. 2013, *The Physics and Evolution of Active Galactic Nuclei* (Cambridge University Press; 1 edition)
- Ni, Q., Brandt, W. N., Luo, B., et al. 2018, *MNRAS*, 480, 5184
- Nikolajuk, M., Czerny, B., Ziółkowski, J., & Gierliński, M. 2006, *MNRAS*, 370, 1534
- Nikolajuk, M., & Walter, R. 2012, *MNRAS*, 420, 2518
- Novikov, I. D., & Thorne, K. S. 1973, in *Black Holes (Les Astres Occlus)*, 343–450
- Onken, C. A., Ferrarese, L., Merritt, D., et al. 2004, *ApJ*, 615, 645
- Page, M. J., Yershov, V., Breeveld, A., et al. 2014, in *Proceedings of Swift: 10 Years of Discovery (SWIFT 10)*, 37
- Pancoast, A., Brewer, B. J., Treu, T., et al. 2014, *MNRAS*, 445, 3073
- Peterson, B. M. 1993, *PASP*, 105, 247
- Peterson, B. M. 2004, in *IAU Symposium, Vol. 222, The Interplay Among Black Holes, Stars and ISM in Galactic Nuclei*, ed. T. Storchi-Bergmann, L. C. Ho, & H. R. Schmitt, 15–20
- . 2014, *SSRv*, 183, 253
- Peterson, B. M., Ferrarese, L., Gilbert, K. M., et al. 2004, *ApJ*, 613, 682
- Plotkin, R. M., Shemmer, O., Trakhtenbrot, B., et al. 2015, *ApJ*, 805, 123
- Polletta, M., Tajer, M., Maraschi, L., et al. 2007, *ApJ*, 663, 81
- Prochaska, J. X., Weiner, B., Chen, H. W., Cooksey, K. L., & Mulchaey, J. S. 2011, *ApJS*, 193, 28
- Runnoe, J. C., Brotherton, M. S., DiPompeo, M. A., & Shang, Z. 2014, *MNRAS*, 438, 3263
- Sadowski, A., Abramowicz, M. A., Bursa, M., et al. 2009, *A&A*, 502, 7
- Schlegel, D. J., Finkbeiner, D. P., & Davis, M. 1998, *ApJ*, 500, 525
- Shakura, N. I., & Sunyaev, R. A. 1973, *A&A*, 500, 33
- Shankar, F., Weinberg, D. H., & Miralda-Escudé, J. 2009, *ApJ*, 690, 20
- Shemmer, O., Trakhtenbrot, B., Anderson, S. F., et al. 2010, *ApJL*, 722, L152
- Shen, Y. 2013, *Bulletin of the Astronomical Society of India*, 41, 61
- Shen, Y., Greene, J. E., Strauss, M. A., Richards, G. T., & Schneider, D. P. 2008, *ApJ*, 680, 169
- Shen, Y., & Ho, L. C. 2014, *Nature*, 513, 210
- Shen, Y., Richards, G. T., Strauss, M. A., et al. 2011a, *ApJS*, 194, 45
- . 2011b, *ApJS*, 194, 45
- Shen, Y., Grier, C. J., Horne, K., et al. 2019, *ApJL*, 883, L14
- Skrutskie, M. F., Cutri, R. M., Stiening, R., et al. 2006, *AJ*, 131, 1163
- Spergel, D. N., Bean, R., Doré, O., et al. 2007, *ApJS*, 170, 377
- Trakhtenbrot, B., & Netzer, H. 2012, *MNRAS*, 427, 3081
- Vestergaard, M., & Osmer, P. S. 2009, *ApJ*, 699, 800
- Vestergaard, M., & Peterson, B. M. 2006, *ApJ*, 641, 689
- Vestergaard, M., & Wilkes, B. J. 2001, *ApJS*, 134, 1
- Wang, J.-G., Dong, X.-B., Wang, T.-G., et al. 2009, *ApJ*, 707, 1334
- Wang, S., Shen, Y., Jiang, L., et al. 2019, *ApJ*, 882, 4
- Wildy, C., Czerny, B., & Kuźmich, A. 2018, *ApJ*, 861, 54
- Wills, B. J., & Browne, I. W. A. 1986, *ApJ*, 302, 56
- Wright, E. L., Eisenhardt, P. R. M., Mainzer, A. K., et al. 2010, *AJ*, 140, 1868
- Wu, J., Brandt, W. N., Anderson, S. F., et al. 2012a, *ApJ*, 747, 10
- Wu, J., Brandt, W. N., Hall, P. B., et al. 2011, *ApJ*, 736, 28
- Wu, X.-B., Hao, G., Jia, Z., Zhang, Y., & Peng, N. 2012b, *AJ*, 144, 49
- Yu, Q., & Tremaine, S. 2002, *MNRAS*, 335, 965
- Yuan, F., & Narayan, R. 2004, *ApJ*, 612, 724